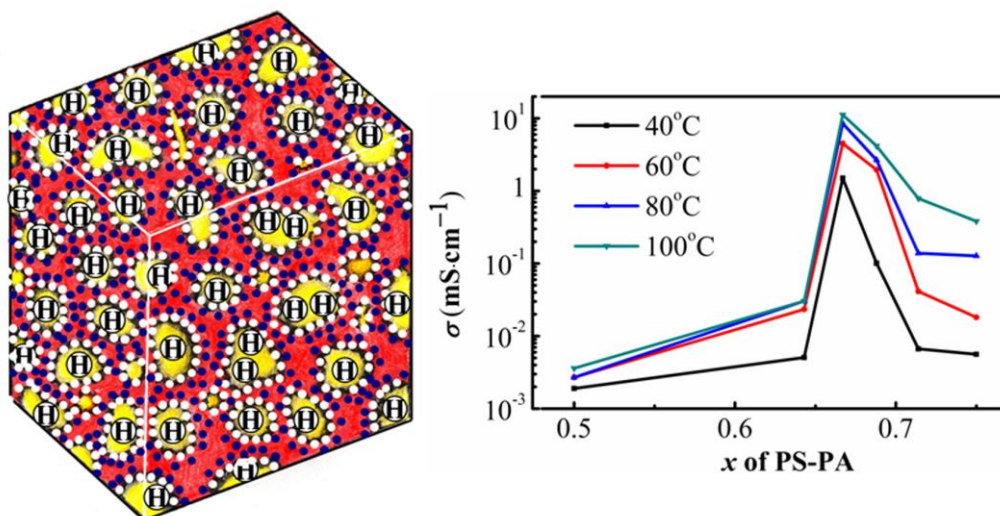# Synergetic Proton Conducting Effect in Acid-Base Composite of Phosphonic Acid Functionalized Polystyrene and Triazolyl Functionalized Polystyrene

Yepei Zhang, Baohua Yue[*], Shuaiyuan Han, and Liuming Yan[*]

Department of Chemistry, College of Sciences, Shanghai University

99 Shangda Road, Shanghai 200444, China

Graphic Abstract

Three orders of magnitude improvement in proton conductivity was observed in the

PS-PA/PS-Tri composite membrane.

[*] Corresponding author.   Tel.: 8621-66132405, fax: 8621-66132405.   E-mail: liuming.yan@shu.edu.cn (L.Y.);

yueyue902@163.com (B.Y.)

Synergetic Proton Conducting Effect in Acid-Base Composite of Phosphonic Acid Functionalized Polystyrene and Triazolyl Functionalized Polystyrene

Yepei Zhang, Baohua Yue[*], Shuaiyuan Han, and Liuming Yan[*]

Department of Chemistry, College of Sciences, Shanghai University

99 Shangda Road, Shanghai 200444, China

ABSTRACT: The synergetic proton conducting effect, three orders of magnitude improvement in proton conductivity, was observed in the acid-base composite composed of phosphonic acid functionalized polystyrene (PS-PA) and triazolyl functionalized polystyrene (PS-Tri). And a new method for the development of proton conducting materials by combination of different acidic and basic polymers is proposed. The PS-PA was synthesized by bromination of polystyrene on the *para*-position of phenyl ring followed by phosphonation and hydrolysis. The PS-Tri was synthesized by chloromethylation of polystyrene on the *para*-position of phenyl ring followed by azidation and 1,3-dipolar cycloaddition or 'click' reaction. Maximum proton conductivity of 11.2 mS cm^{-1}, which is three orders of magnitude higher than that of pristine PS-PA or PS-Tri, and tensile strength of 16.3 MPa, as well as a minimum water uptake of 15.1% (90 °C, 90% RH), were observed in the PS-PA/PS-Tri composite composed of 66.7% PS-PA. Finally, a mosaic-like morphology model and space-charge effect were proposed to explain the synergetic proton conducting effect.

KEYWORDS: proton conducting material; synergetic proton conducting effect; mosaic-like morphology model; phosphonic acid functionalized polystyrene; triazolyl functionalized

---

[*] Corresponding author. Tel.: 8621-66132405, fax: 8621-66132405. E-mail: liuming.yan@shu.edu.cn (L.Y.); yueyue902@163.com (B.Y.)

polystyrene; acid-base composite

1. INTRODUCTION

With the increasingly serious environment pollution and energy consumption, there is rising interest to exploit novel and renewable energy resources to substitute fossil fuels including nature gas, petroleum, and coal, or to develop new energy technologies utilizing fossil fuels more cleanly and efficiently. Among the many technologies, fuel cells, which convert chemical energy directly into electrical energy without combustion, are considered to be competitive energy conversion technologies owing to their environmental friendliness and high efficiency.[1] Especially, proton exchange membrane fuel cells (PEMFCs) are believed to be a real green energy technology as PEMFCs consume only hydrogen and air and release only water.[2, 3] As a matter of fact, PEMFCs have been found potential applications in transportation and as portable and stationary power sources because of their low operation temperature, high power density, high conversion efficiency, long service life, and high reliability.[4-8]

However, the large-scale commercialization of PEMFCs depends greatly on the cost affordability and the supply, distribution, and storage technologies of hydrogen. As one of the two essential materials of PEMFCs, proton exchange membrane (the other material is electrocatalyst) is not only a major origin of high cost of PEMFCs, but also a technological bottleneck of high-temperature PEMFCs (HT-PEMFCs).[9-12] For example, the HT-PEMFCs possess significant advantages compared to low to medium temperature PEMFCs since the electrocatalyst activity, especially its tolerance to impurities in fed-gas, is greatly enhanced at high temperature thus the supply obstacle of hydrogen can be overcome.[13-15] However, the development of HT-PEMFCs relies on the development of high-temperature proton exchange

membranes possessing high proton conductivity to support high current, adequate mechanical strength and stability, chemical and electrochemical stability under operation conditions, and reasonable price for the large-scale commercialization.[11, 16, 17]   Though the most widely accepted proton exchange membranes based on perfluorosulfonic acid, such NAFION, could meet almost all these characteristics except reasonable price for low to medium temperature application, the proton conductivity degradation at high temperature and dehydrated state has hindered their application in HT-PEMFCs.[18, 19]   Therefore, it is important to search for proton exchange membranes with high performance at elevated temperature and under dehydrated or even anhydrous states.

In the search for high temperature proton exchange membranes, a new type of proton exchange membranes based on acid-base composite have attracted great attention for their improved proton conductivity at elevated temperature and under dehydrated or even anhydrous states.[20]   In an acid-base composite, the base component plays as hydrogen-bonding (H-bonding) acceptor and acid component as H-bonding donor.   In addition, the H-bonding bridges provide proton transport pathways under dehydrated states, and the ionic cross-linking between acidic groups and basic groups depresses the water uptake and swelling and improves the mechanical properties.

For example, Liang et al. developed an acid-base composite membrane composed of sulfonated polymers as acidic components and polyetherimide (PEI) as basic components showing better resistance to swelling and improved thermal stability, but slightly reduced proton conductivity compared to the corresponding pristine sulfonated polymers.[21]   Fu et al. prepared an acid-base composite membrane by blending polysulfone bearing benzimidazole side groups with sulfonated SPEEK, exhibiting better performance in PEMFC at 90 and 100 ℃ compared to

the pristine SPEEK and NAFION 111 membranes.[22] Kufacı synthesized a novel anhydrous

proton conducting polymer electrolyte based on poly(ethyleneglycol methacrylate phosphate)

(PEGMAP) and heterocycle and obtained a proton conductivity of 0.2 mS cm^{-1} at 160 °C and

anhydrous states.[23] Wu et al. blended sulfonated poly(2,6-dimethyl-1,4-phenylene oxide) with

(3-aminopropyl)triethoxylsilane through a sol-gel process resulting high proton conductivity and

low methanol permeability as compared to NAFION 117.[24]

For the preparation of acid-base composite proton exchange membranes, two types of

polymers, the phosphonic acid functionalized and nitrogenous heterocyclyl functionalized

polymers, have attracted great attention as potential functional polymers because of their

chemical and thermal stability, versatile hydrogen-bonding formation ability, and potential high

proton conductivity. The phosphonic acid possesses not only improved thermal and chemical

stability, but also shows improved proton conductivity at high temperature under anhydrous

states compared to sulfonic acid.[25-27] The nitrogenous heterocycles or immobilized

nitrogenous heterocycles were firstly proposed to substitute water as H-bonding formation

solvent at high temperature to avoid the evaporation of solvent owing to their high boiling point

temperature.[9, 28] Based on these arguments, Yan et al. studied the hydrogen bonding and

proton transport characteristics of complexes composed of phosphonic acid and nitrogenous

heterocycles by density functional theory calculations, molecular dynamics simulations, and ^{1}H

NMR spectroscopy, and proposed and verified the possible synergetic proton transport in

acid-base complexes or composites.[29-31] Bozkurt et al. prepared a series of acid-base

composite membranes by blending poly(vinylphosphonic acid) (PVPA) with

poly(1-vinylimidazole) (PVIm),[32] poly(1-vinyl-1,2,4-triazole),[33] poly(2,5-benzimidazole)

(ABPBI),[34] and so on, and satisfactory results were obtained.

In this paper, acid-base composite proton exchange membranes will be prepared based on phosphonic acid functionalized and triazolyl functionalized polystyrene. The ^{1}H NMR spectroscopy will be applied to characterize molecular structures, and thermogravimertric analysis to characterize thermal stability. The synergetic proton conducting effect in the acid-base composite is observed, and a new method for the development of proton conducting materials is proposed.

## 2. EXPERIMENTAL SECTION

2.1 Materials

Polystyrene (PS) was purchased from Aladdin Reagent Inc. with a molecular weight of 100,000 and used as received. Zinc chloride ($ZnCl_2$, Sinopharm Chemical Reagent Co., Ltd (SCRC), > 98%) was dehydrated in thionyl chloride ($SOCl_2$, SCRC, > 99%) at 85 ℃ under reflux for 1 hour. Chloroform ($CHCl_3$, SCRC, > 99%) was pretreated before use according to the following process: washed using sulfuric acid (H_2SO_4, SCRC, 95% - 98%) and deionized water repeatedly for three times, dried by anhydrous calcium chloride ($CaCl_2$, Aladdin Reagent Inc.), and finally distilled. Sodium ascorbate (NaAsc, 99%), liquid bromine (Br_2), anhydrous ferric chloride ($FeCl_3$), sodium azide (NaN_3), and 2-methyl-3-butyn-2-ol were purchased from Aladdin Reagent Inc. and used as received. Diethyl phosphate (DEP, 99%), diphenyl ether (DPE), *N*,*N*-dimethylformamide (DMF), triethylamine (Et$_3$N, > 99%), copper sulfate pentahydrate ($CuSO_4$ $5H_2O$, > 99%), and hydrochloric acid (HCl, 36 - 38%) were provided by SCRC and used as received. Tris(dibenzylideneacetone) dipalladium adduct ($Pd_2(dbac)_3$) was provided by Yurui Reagent Inc. and used as received. Chloromethyl methyl ether ($ClCH_2OCH_3$) was purchased from Shanghai Jiyan Chemical Reagent Co. and used as received.

2.2 Bromination of PS

The bromination of PS was carried out based on the procedure as reported by Subianto et al.[35]   PS (2.8848 g) and anhydrous $FeCl_3$ (0.3165 g) were firstly added in a flask equipped with a reflux column and a magnetic stirrer.   And then, 30 mL $CHCl_3$ was added to dissolve these materials.   Thirdly, 1.5 mL bromine (dissolved in 20 mL $CHCl_3$) was added very slowly (in about 15 minutes) because of the extremely exothermic of the reaction.   The reaction mixture was kept in dark, protected under continuous N_2 flow, and stirred for 2 h at 60 ℃.   In the end of the reaction, the reaction mixture was poured into methanol, and the precipitated polymer was recovered as product (PS-Br).   The PS-Br was further dissolved in 1,2-dichloroethane and reprecipitated in methanol to wash out any residual bromine.   Finally, the PS-Br was filtered and dried at 60 ℃ in vacuum oven overnight, and 3.0596 g white powder was obtained (yield 60.1%).

^{1}H NMR (500 MHz, $CDCl_3$, δ): 7.26 - 6.86 (meta- and para-aromatic *H*, *PS + substituted* PS), 6.86 - 6.18 (ortho-aromatic *H*, *PS + substituted* PS), 1.75 (-C*H*(Ar)-), 1.41 (-C*H$_2$*-).
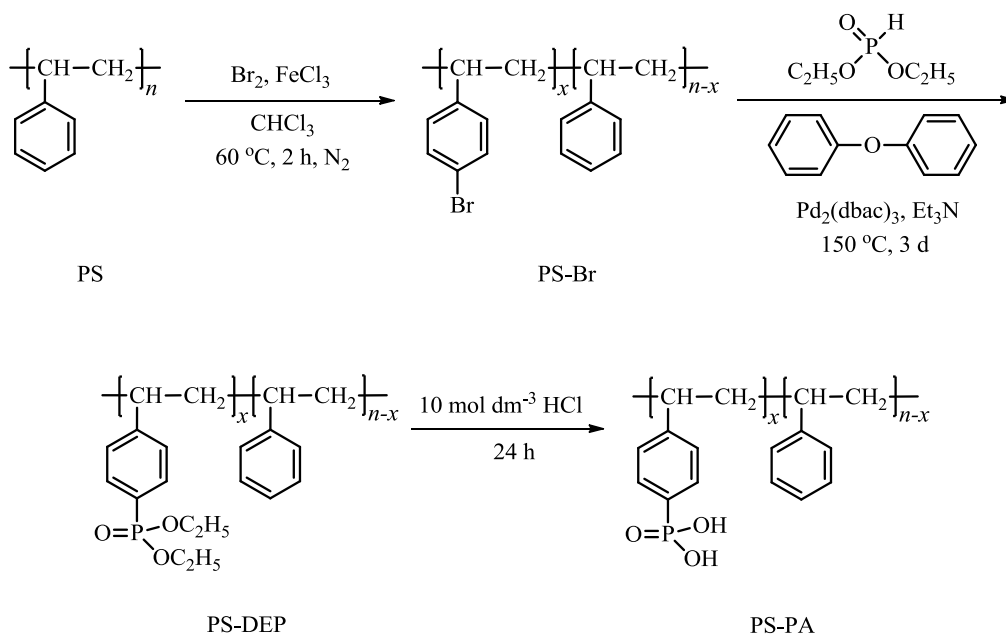
Scheme 1. The synthesis of phosphonic acid functionalized PS

2.3 Phosphonation of PS-Br

Firstly, 1.0252 g PS-Br was dissolved in diphenyl ether (12 mL) in a flask fitted with gas inlet and outlet. And then, Et_3N (0.5 mL), DEP (6 mL), and $Pd_2(dbac)_3$ (0.0426 g) were injected successively into the flask under flowing N_2. Thirdly, the reaction solution was stirred at 150 ℃ for 3 days under continuous N_2 flow. Finally, the phosphonated PS (PS-DEP) was precipitated in a 95/5 v/v methanol/water solution, isolated as a pale yellow solid, and dried under vacuum at 60 ℃ for 1 day with a yield of 78 % (1.0379 g).

^{1}H NMR (500 MHz, $CDCl_3$, δ): 7.26 - 6.86 (meta- and para-aromatic *H*, *PS + substituted* PS), 6.84 - 6.00 (ortho-aromatic *H*, *PS + substituted* PS), 4.16 (-O-C*H2*-), 2.25 - 1.60 (-C*H*(Ar)-), 1.60 - 1.25 (-C*H2*-, -C*H3*).

2.4 Hydrolysis of PS-DEP

Firstly, 0.4457 g PS-DEP was added in 10 mol dm^{-3} HCl (50 mL) and stirred at 100 ℃ for

24 h.   And then, the product was washed by deionized water for three times to eliminate any residual free acid.   Finally, the product was dried at 60 ℃ in a vacuum oven for 12 h, and 0.3429 g (yield 77%) phosphonic acid functionalized polystyrene (PS-PA) was obtained.

^{1}H NMR (500 MHz, DMSO-d$_6$, δ): 7.33 - 6.87 (meta- and para-aromatic H, PS + $substituted$ PS), 6.87 - 6.36 (ortho-aromatic H, PS + $substituted$ PS), 3.26 - 3.17 (-OH-), 1.86 - 1.00 (-CH(Ar)-, -CH_2-).

2.5 Chloromethylation of PS

Firstly, 2.1327 g of PS and 5.5780 g of anhydrous ZnCl$_2$ were added in 100 mL pretreated CHCl$_3$ under N$_2$ protection in a flask equipped with gas inlet and outlet, a reflux column, and a magnetic stirrer.   After the PS was completely dissolved, 7 mL of ClCH$_2$OCH$_3$ ($n_{ZnCl_2} : n_{ClCH_2OCH_3} : n_{PS} = 2:5:1$; n_{PS} represents the moles of repeat unit of PS) was added into the solution.   And then, the reaction was proceeded at 60 ℃ for 7 h and a pink solution was obtained.   The pink solution was precipitated in a 9 : 1 v/v methanol/water mixture, and white flocculent precipitate was recovered.   Finally, the precipitate was redissolved in CHCl$_3$, and reprecipitated in methanol/water mixture for 3 times.   The resulting polymer (PS-CH$_2$-Cl) was dried in a vacuum oven at 60 ℃ for 24 h with a yield of 74 % (2.3161 g).

^{1}H NMR (500 MHz, CDCl$_3$, δ): 7.29 - 6.86 (meta- and para-aromatic H, PS + $substituted$ PS), 6.86 - 6.36 (ortho-aromatic H, PS + $substituted$ PS), 4.55 - 4.42 (Ar-CH_2-Cl), 1.80 - 1.28 (-CH(Ar)-, -CH_2-).
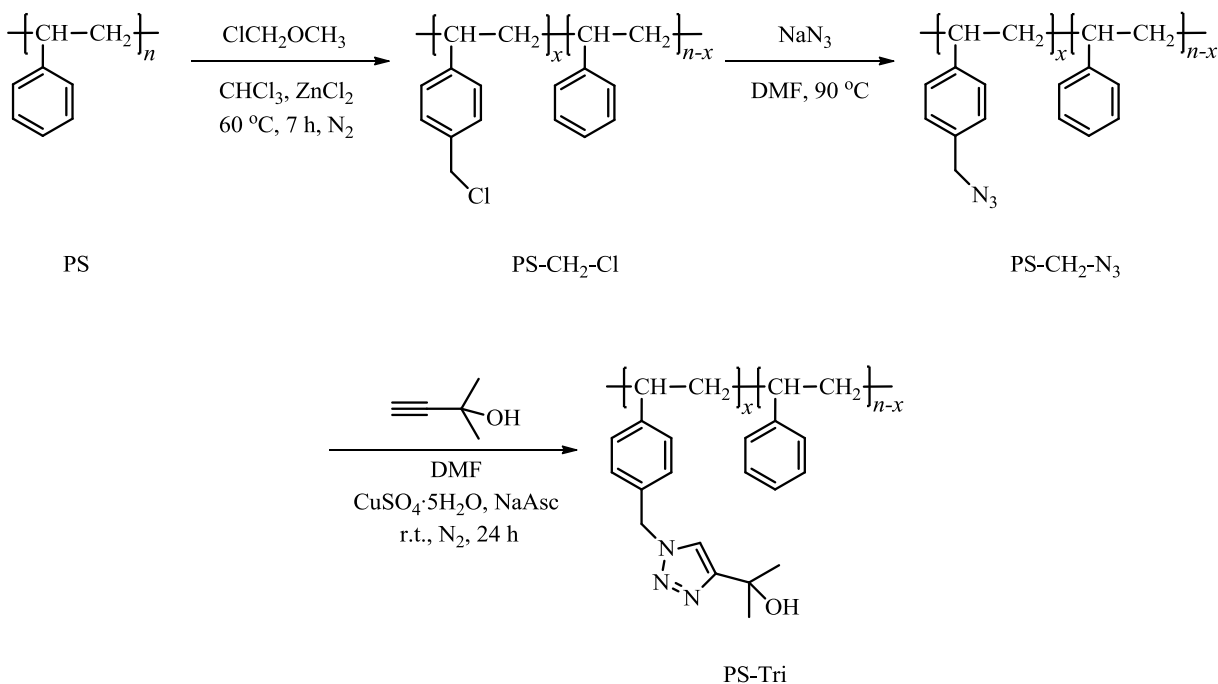
Scheme 2. Triazolyl functionalization of PS

2.6 Azidation of PS-CH₂-Cl

PS-CH₂Cl (0.9683 g) and excess NaN₃ (0.5183 g) were mixed in 25 mL DMF and stirred at 90 °C for 12 h. The product was precipitated in water yielding a pale yellow solid (PS-CH₂-N₃, 0.8951 g, yield 89%) and washed for three times in water to remove the excess NaN₃.

^{1}H NMR (500 MHz, CDCl₃, δ): 7.26 - 6.81 (meta- and para-aromatic *H*, *PS + substituted PS*), 6.82 - 6.44 (ortho-aromatic *H*, *PS + substituted* PS), 4.21 - 4.20 (Ar-C*H₂*-N₃), 1.78 - 1.74 (-C*H*(Ar)-), 1.54 - 1.40 (-C*H₂*-).

2.7 The 'click' reaction

PS-CH₂-N₃ (0.8951 g, 1.0 equiv.), 2-methyl-3-butyn-2-ol (0.5309 g, 1.1 equiv.), CuSO₄ 5H₂O (0.2067 g, 0.1 equiv.), and NaAsc (0.3615 g, 0.3 equiv.) were dissolved in 20 mL DMF and stirred at room temperature for 24 h under N₂ protection. The yellow solution was then precipitated in water and dried yielding 1.1032 g triazolyl functionalized PS (PS-Tri) at a

yield of 92%.

^{1}H NMR (500 MHz, DMSO-d$_6$, δ): 7.95 (N-CH=C), 7.12 - 6.72 (meta- and para-aromatic H, *PS* + *substituted* PS), 6.72 - 6.34 (ortho-aromatic H, *PS* + *substituted* PS), 5.44 - 5.40 (Ar-CH_2-N), 5.14 - 5.12 (-OH), 1.71 - 1.27 (-CH(Ar)-, -CH_2-, -C(CH_3)$_2$).

2.8 Preparation of acid-base composite membranes

The PS-PA and PS-Tri were firstly ground into tiny powders separately, and then mixed

$(\dfrac{n_{\text{PS-PA}}}{n_{\text{PS-PA}} + n_{\text{PS-Tri}}} \times 100\%$ = 0.0%, 50.0%, 64.3%, 66.7%, 68.7%, 71.4%, 75.0%, 100.0%, where

$n_{\text{PS-PA}}$ and $n_{\text{PS-Tri}}$ represent the moles of phosphonic acid group and triazolyl group, respectively). Finally, the mixed powders were hot-pressed using a FM1202 vacuum pressing machine at 160 ℃ for 30 minutes under evacuation.

2.9 Characterizations Methods

2.9.1 ^{1}H NMR Spectroscopy

The molecular structures of the polymers were characterized by ^{1}H NMR spectroscopy on a Bruker Avance 500 MHz NMR spectrometer using tetramethylsilane (TMS) as internal reference and CDCl$_3$ or DMSO-d$_6$ as solvent.

2.9.2 Proton Conductivity

The proton conductivity was measured by two-electrode impedance spectroscopy (rounded Pt electrodes with diameter of 6 mm) at 90% relative humidity in a KR-K humidity-temperature controller using a Solartron 1255B response analyzer. In order to establish hydration equilibrium, the membranes were kept in the humidity-temperature controller preset at measurement temperature and humidity for at least four hours before each measurement. All the experimental impedance spectra were fitted to the equivalent circuit as shown in **Figure 1**, where R_0 represents the membrane resistance, R_1 and R_2 are interface resistances, CPE_1 and

CPE_2 are constant phase elements, and L_0 is inductance (it is significant only at high frequency). And the conductivity of the membrane is calculated as, $\sigma = d / R_0 A$, where d and A are thickness and area of the membrane between two electrodes. In **Figure 1**, it also shows two of the typical experimental impedance spectra and their corresponding fitted impedance spectra with satisfactory fitting results. In **Table 1**, it summarized the fitted parameters of the impedance spectra in **Figure 1** as examples.
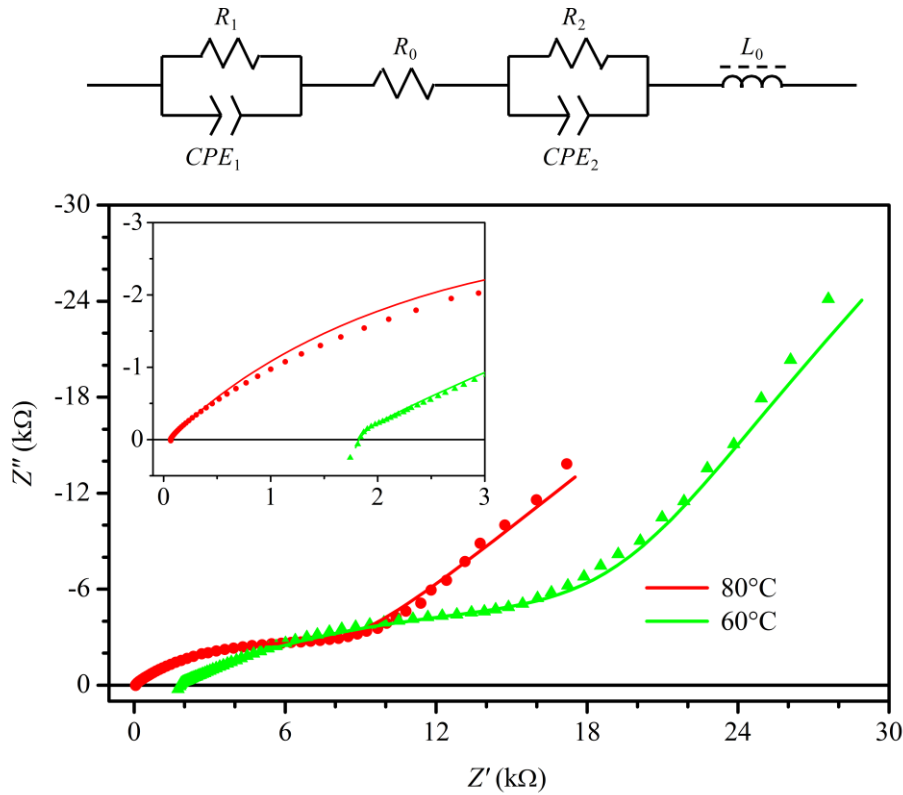

Figure 1. The equivalent circuit and typical impedance spectra, the curves represent the fitted impedance spectra and data points represent of the experimental results

Table 1. Fitted parameters to the equivalent circuit, Q and n are parameters for the constant

phase elements with $Z_{CPE} = \dfrac{1}{Q\omega^n} \exp(-j\dfrac{\pi}{2}n)$

T ($^{\circ}$C)	60	80
L_0 (μH)	32.46	4.94
R_0 (Ω)	1821	63.6
R_1 (kΩ)	22.270	7.521
Q_1 (μS$\cdot$s^{n_1})	9.654	4.579
n_1	0.415	0.631
R_2 (kΩ)	197.2	8.9×10^{11}
Q_2 (μS$\cdot$s^{n_2})	61.01	80.12
n_2	0.857	0.577

2.9.3 Mechanical Property

The mechanical properties of the membranes were characterized using a MTF-100 microcomputer controlled electronic micro-tensile machine stretched at constant speed of 0.1 mm min^{-1}.   The tensile strength was evaluated as ultimate tensile strength at break at 25 $^{\circ}$C in air.

2.9.4 Thermogravimetric Analysis (TGA)

TGA was carried out in nitrogen atmosphere from 33 to 500 ℃ at a heating rate of 10 ℃ min^{-1}.   All the samples were pre-heated at 60 ℃ overnight before testing.

2.9.5 Water Uptake

During the measurement of water uptake, the membranes were firstly dried in an oven at 110 ℃ for 12 hours, and then weighed (w_d), respectively.   The weighed membranes were left in a

humidity-temperature controller at 90% relative humidity and preset temperature overnight. After taken from the humidity-temperature controller, the membrane was weighed (w_w) quickly and the water uptake (w_u) was evaluated as $w_u = \dfrac{w_w - w_d}{w_d} \times 100\%$.

3. RESULTS AND DISCUSSION

3.1 ^{1}H NMR spectroscopy and degree of substitution

The ^{1}H NMR spectra of PS, PS-Br, and PS-DEP were shown in **Figure 2**. For the ^{1}H NMR spectrum of PS, the broad peak at 6.95 - 6.31 ppm is from the ortho-aromatic proton H_o and the peak at about 7.27 - 6.95 ppm from the meta- and para-aromatic protons H_m and H_p of the phenyl ring. After bromination and phosphonation, these peaks slightly shift to 6.86 - 6.18 ppm and 7.26 - 6.86 ppm, or to 6.84 - 6.00 ppm and 7.26 - 6.84 ppm, respectively. For the PS-DEP, a new peak appears at 4.16 ppm attributing to the -OCH_2- of the ethoxyl group, and the peak of the -CH_3 of the ethoxyl group appears at the same range as the -CH_2- of the polymer backbone at 1.60 - 1.25 ppm. In addition, the peaks of aromatic H_m and H_p for PS-DEP, which overlap for PS and PS-Br, split into two groups of peaks because of the existence of ^{31}P nearby. From the ^{1}H NMR spectra of PS-DEP and PS-PA in DMSO-d_6 as shown in **Figure 3** (PS-PA does not dissolve in CDCl$_3$, and the ^{1}H NMR of PS-DEP in DMSO-d_6 is slightly different from that in CDCl$_3$), the peak at 3.95 ppm attributing to the -OCH_2- of the ethoxyl group disappears and the peak at 3.26 - 3.17 ppm attributing to the hydroxyl group, which overlaps the peak of water, confirms the complete hydrolysis of PS-DEP.[36]
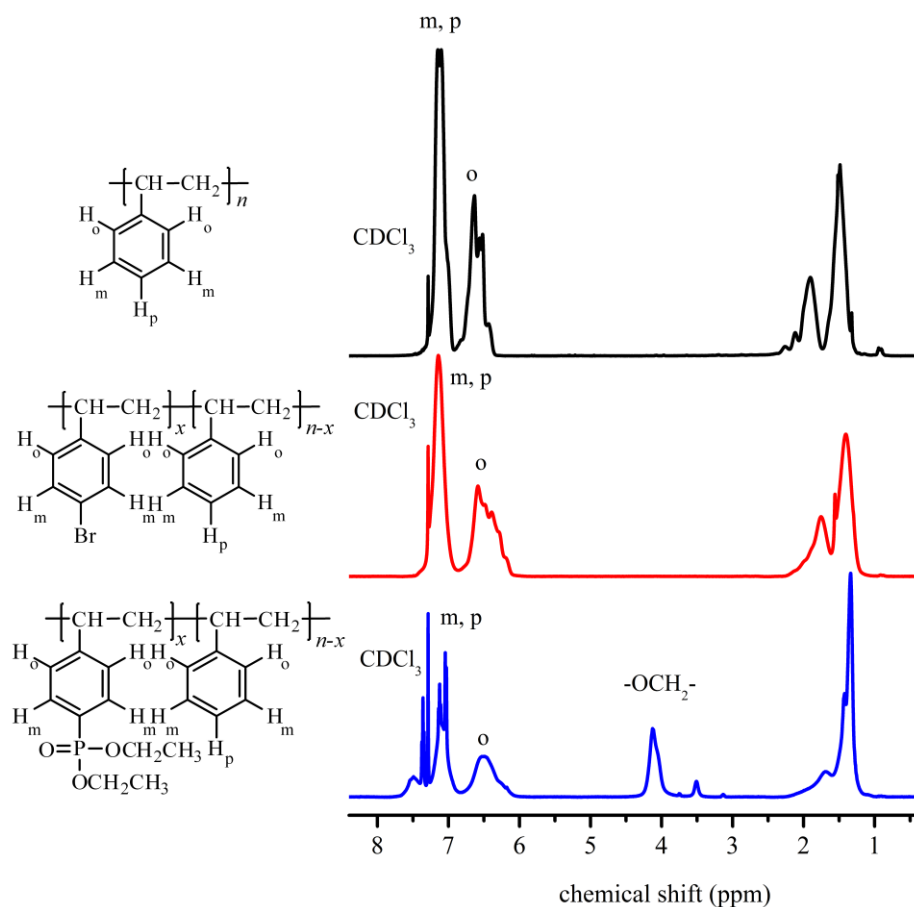
Figure 2. ^{1}H NMR spectra of PS, PS-Br, and PS-DEP dissolved in CDCl$_3$.

The degree of bromination DB (or phosphonation DP), the number of Br atoms (or phosphonic acid groups) grafted per repeat unit of PS, was evaluated by peak integration of the corresponding ^{1}H NMR spectrum. Firstly, the peak integration from the ortho-aromatic protons H_o was normalized to 2, and then, the peak for meta- and para-aromatic protons H_m and H_p was integrated as $I_{m,p}$. The degree of bromination DB was calculated as DB = 3 - $I_{m,p}$. The degree of phosphonation DP was evaluated by peak integration from the -OCH_2- units at 4.16 ppm with DP = $I_{ethoxyl}$ / 4.

15

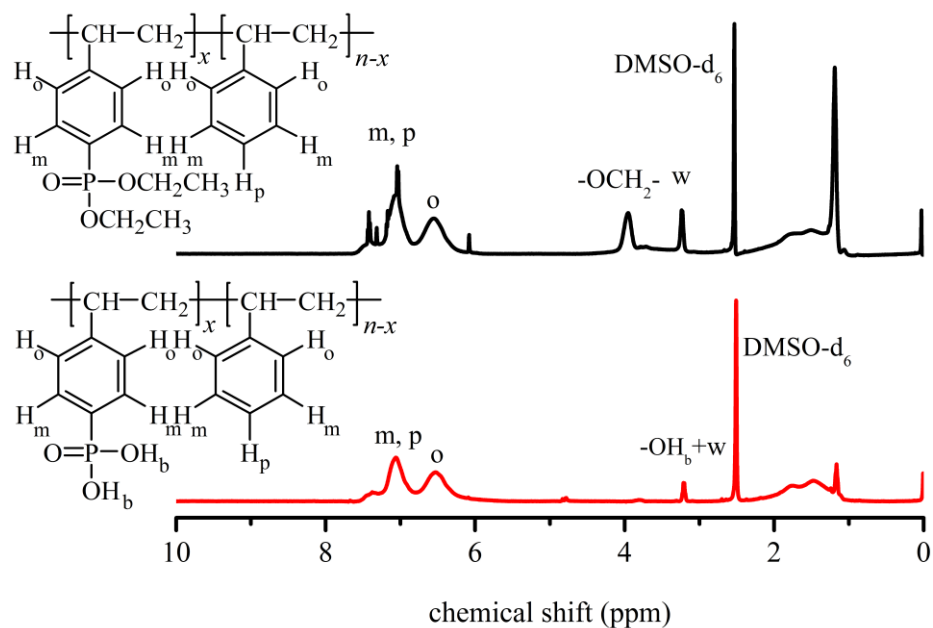**Figure 3.** ^{1}H NMR spectra of PS-DEP and PS-PA dissolved in DMSO-d$_6$.

In **Figure 4**, it shows the ^{1}H NMR spectra of PS, PS-CH$_2$-Cl, PS-CH$_2$-N$_3$, and PS-Tri. The ^{1}H NMR for PS-CH$_2$-Cl shows three broad peaks, respectively, at 6.86 - 6.36 ppm attributing to the ortho-aromatic proton H_o, at 7.29 - 6.86 ppm to the meta- and para-aromatic protons H_m and H_p, at 4.55 - 4.42 ppm to the Ar-CH$_2$-Cl protons H_b. These peaks slightly shift to 6.81 - 6.44 ppm, 7.26 - 6.81 ppm, and 4.21 - 4.20 ppm after azidation, and shift further to 6.72 - 6.34 ppm, 7.12 - 6.72 ppm, and 5.44 - 5.40 ppm after "click" reaction.

The degree of chloromethylation, DC, the number of chloromethyl groups grafted per repeat unit of PS, was evaluated from peak integration of the peak at 4.55 ppm (I_b) for PS-CH$_2$-Cl, DC $= I_b / 2$. The degree of triazolylation, DT, the number of triazolyl groups grafted per repeat unit of PS, was evaluated from peak integration of the methyl protons around 1.4 ppm (I_{methyl}) for PS-Tri, $DT = (I_{methyl} - 3)/6$.
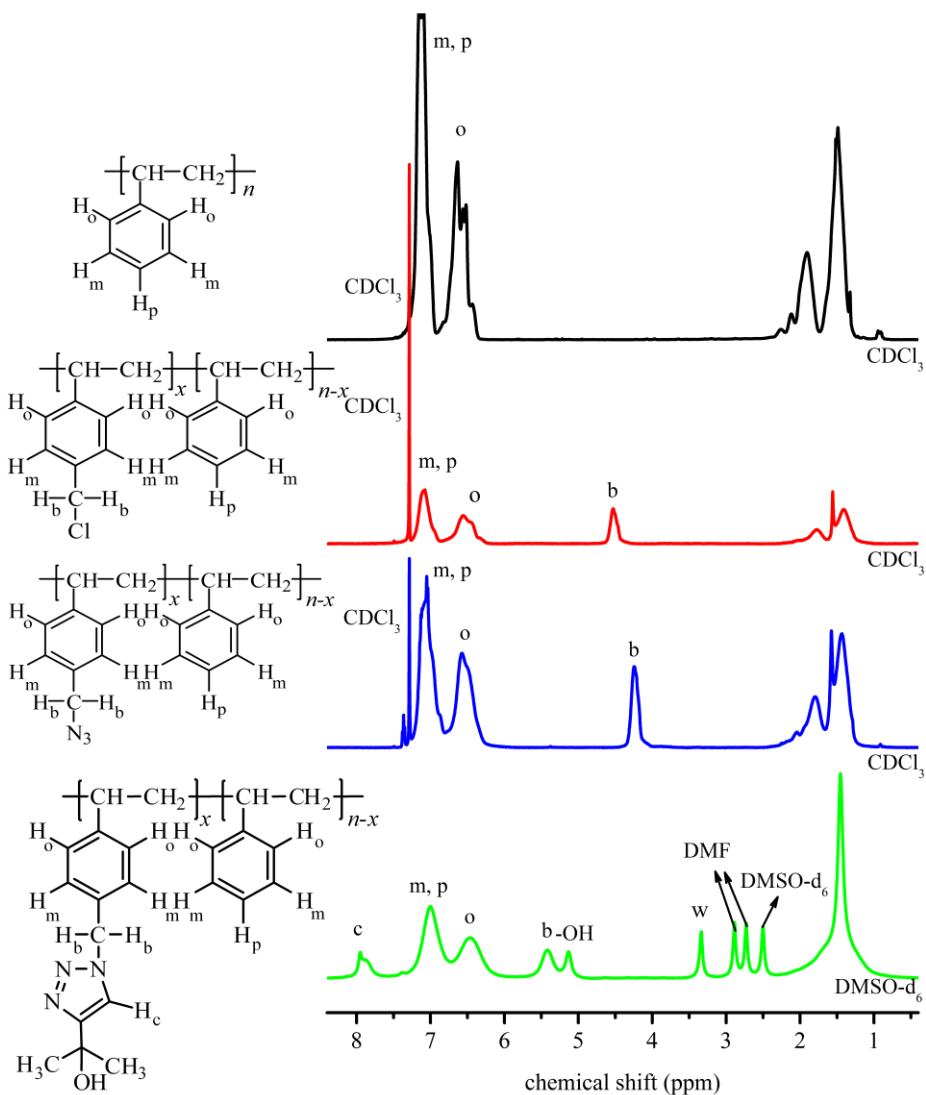
16

Figure 4. ^{1}H NMR spectra of PS, PS-CH$_2$Cl, and PS-CH$_2$N$_3$ in CDCl$_3$, and PS-Tri in DMSO-d$_6$.

As a catalyzed reaction, bromination degree depends on the amount of catalyst used. When the mass ratio of catalyst to PS increases from 0.068 to 0.095, the degree of bromination increases from 0.36 to 0.51 (**Table 2**). In the same way, the degree of phosponation depends on the amount of catalyst used during the phosphonation reaction. When the molar ratio of catalyst to repeat unit of PS increases from 8.0×10^{-3} to 9.2×10^{-3}, the degree of phosphonation

increases from 0.36 to 0.43 (**Table 2**), which is significantly higher than literature value at 0.33.[35]

The chloromethylation of PS is extremely sensitive to moisture, and the whole reaction must be operated under anhydrous state. The highest degree of chloromethylation, DC, is 60% in this work, and the degree of triazolylation, DT, is almost equivalent to DC due to the completeness of the 'click' reaction.

Table 2. Degrees of bromination and phosphonation

Catalyst*	t (h)	DB	Catalyst†	t (h)	DP
0.068	2	0.36	8.0×10^{-3}	72	0.36
0.071	2	0.47	8.9×10^{-3}	72	0.38
0.095	2	0.51	9.2×10^{-3}	72	0.43

* mass ratio of catalyst to PS.   † molar ratio of catalyst to repeat unit of PS.

3.2 Proton conductivity

In **Figure 5**, it shows the impedance spectroscopy of a membrane (composed of 66.7% PS-PA) measured at 10 mV, 20 mV, and 30 mV, respectively under 100 ℃ and 90% relative humidity. It is obvious that the impedance spectroscopy is almost invariant especially at high frequency revealing the linear relationship between current and voltage (ohmic behavior) of the membrane.
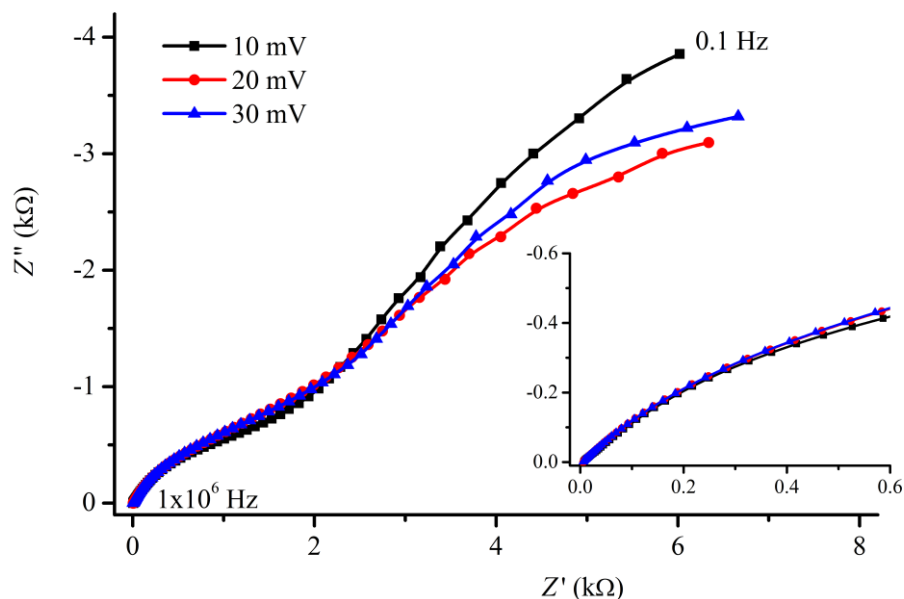
Figure 5. The impedance spectroscopy of the 66.7% PS-PA membrane measured at different voltage (100 ℃, RH 90%, 10^6 - 0.1 Hz).

The proton conductivities of pristine PS-PA and PS-Tri are very low at about 10^{-3} mS cm^{-1}. For the acid-base composites of PS-PA and PS-Tri, the proton conductivities are greatly improved (**Figure 6**). The equimolar acid-base composite, composed of 50.0% PS-PA, shows very low conductivity at about 2×10^{-3} mS cm^{-1}. If more acidic component is added to the composite, a synergetic proton conducting effect, the proton conductivity of the acid-base composite improves remarkably compared with both the acidic component and the basic component, is observed. And the maximum proton conductivity, three orders of magnitude improvement, is observed in the composite composed of 66.7% PS-PA (PS-PA : PS-Tri = 2 : 1) at 11.2 mS cm^{-1} (100 ℃ and RH 90%). However, the proton conductivity decreases when the PS-PA component exceeds 66.7%.

The proton conductivity is also dependent on temperature, the proton conductivity at 40 ℃ is approximately one order of magnitude lower than that at 100 ℃ revealing an activation
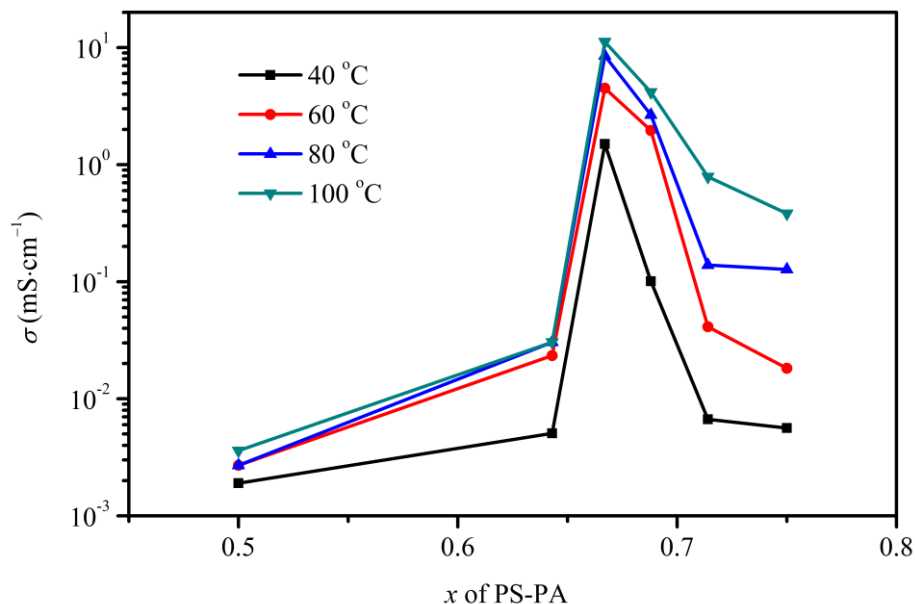
process of proton conducting in the acid-base composites.

Figure 6. The proton conductivities of the composites of PS-PA and PS-Tri.

3.3 Thermal stability of PS-Tri and PS-PA

The TGA (**Figure 7**) shows that PS-PA undergoes 3.5 wt% initial mass loss below 191 ℃ attributing to the evaporation of water, and then, 8.3 wt% additional mass loss attributing to the formation of anhydride by creation of P-O-P linkages and the evaporation of low molecular weight materials below 312 ℃.[37] Between 312 ℃ and 414 ℃, the PS-PA is stable and there is only insignificant mass loss. Finally, in the narrow temperature range from 414 ℃ to 443 ℃, large mass drop, with only about 35.5 wt% residual mass left, is observed attributing to the decomposition of PS-PA.

The PS-Tri is thermally stable up to 267 ℃ under N_2 protection attributing to the aromatic structure. And the mass loss below 267 ℃ is attributed to the loss of physisorbed and chemisorbed water, and other low molecular weight masses. The decomposition starting at 267

℃ until 385°C is attributed to the loss of triazolyl group.　And final decomposition starts at 385 °C and finishes at 444 ℃ with only about 37.3 wt% total mass left.
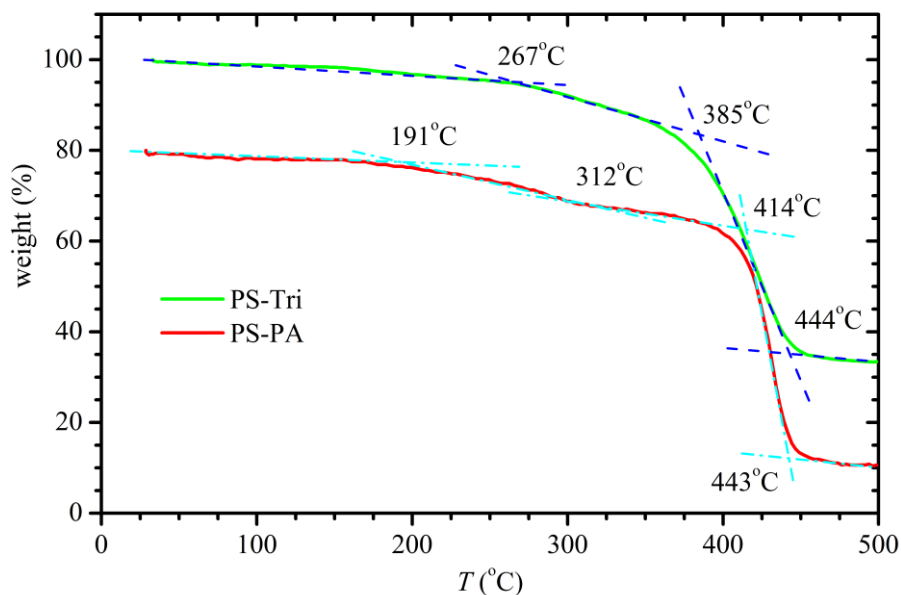

Figure 7. The thermogravimetric analysis of the PS-Tri and PS-PA, notice that the PS-PA curve is offset down by 20 wt% for clarity.

3.4 Water uptake

In **Figure 8**, it summarizes the water uptake of the acid-base composite membranes, as well as the acid and the base components at temperatures between 40 to 100 ℃ and at relative humidity of 90%.　The phosphonic acid group and triazolyl group are highly hydrophilic, and thus exhibit greater water uptake than the composite membranes.　As the base component PS-Tri is composited into the PS-PA, its hydrophilicity decreases significantly and a lowered water uptake of 15.1% at 100 °C and 90% RH is observed in the PS-PA/PS-Tri membrane containing 66.7% PS-PA.

At constant component, the water uptake increases with temperature and the highest water
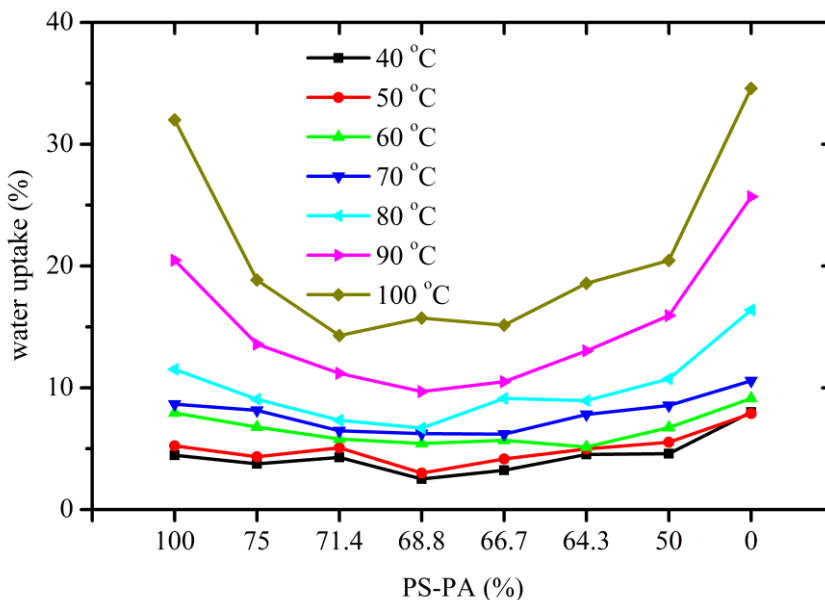
uptake 34.6% is observed at 100 ℃ for PS-Tri.

Figure 8. Water uptake of the acid-base composite membranes (40 - 100 $^{\circ}$C, 90% RH).

3.5 Mechanical property

Tensile characteristics of pristine PS-PA, PS-Tri, and acid-base composites (dry membranes) are shown in **Figure 9**.   The tensile strengths at break for pristine PS-PA and PS-Tri are 15.1 MPa and 12.6 MPa, respectively, with the acidic PS-PA significantly better than the basic PS-Tri attributing to the formation of anhydride by creation of P-O-P linkages and thus resulting compact structure.[38]

The acid-base composite composed of 50% PS-PA shows a tensile strength at 12.9 MPa which is between the pristine acidic PS-PA and basic PS-Tri components.   For the composite composed of 66.7% PS-PA, a tensile strength of 16.3 MPa is observed showing significant synergetic effect owing to the ionic-bridges between the phosphonic acid groups and the triazolyl groups.

22

The tensile moduli at zero stress are 39.8 and 22.6 MPa for PS-PA and PS-Tri, respectively. For the equimolar PS-PA and PS-Tri composite, the tensile modulus increases to 49.0 MPa, showing significant ionic interaction between these two components. As more acidic component PS-PA is blended into the composite, the tensile modulus decreases to 34.3 MPa in the 66.7% PS-PA.

The improvement in mechanical properties in the PS-PA/PS-Tri composite may be attributed to the ionic cross-links between the acid groups and base groups, however, the number of ionic cross-links, depending on the completeness of mixing of the interaction groups, is sensitive to the preparation process of the composite. We have to admit that the mechanical properties of the composites are sensitive to the preparation process and often vary from batch to batch in our experiments; therefore, these results are not conclusive.
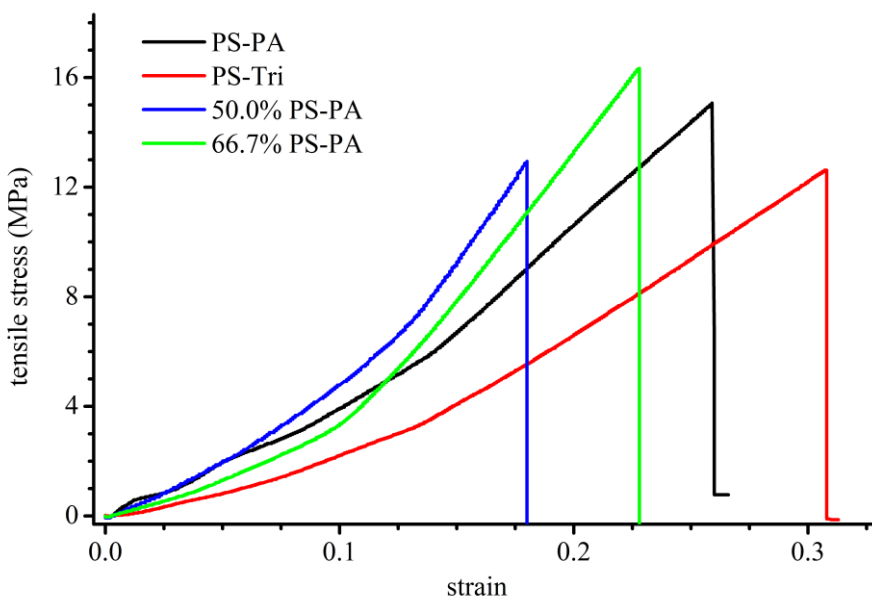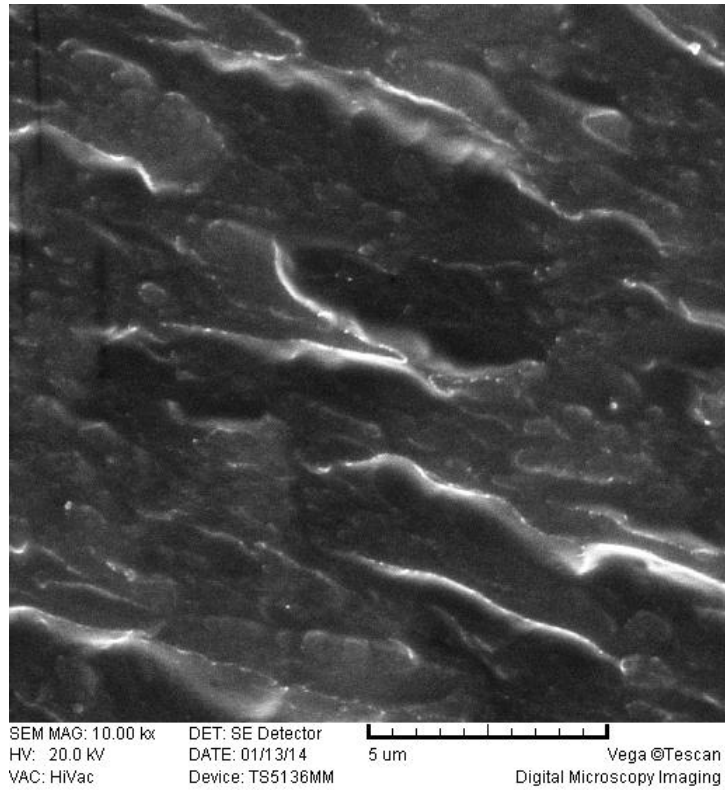

Figure 9. Tensile characteristics of pristine PS-PA and PS-Tri, and the acid-base composites (dry membranes).
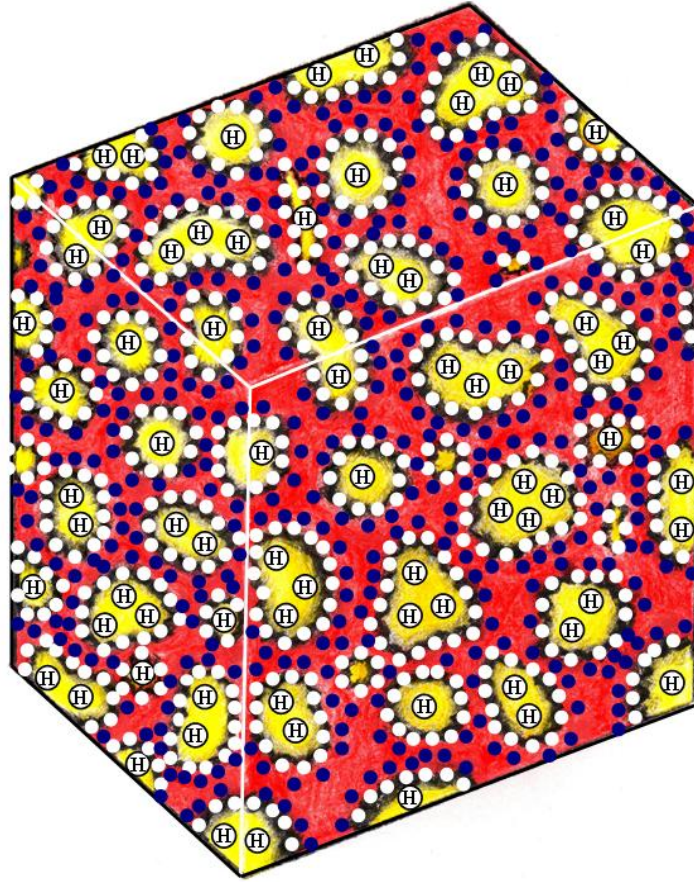
3.6 Mosaic-like morphology model

Although both phosphonic acid groups and triazolyl groups are amphoteric and can self-dissociate resulting relatively high proton conductivity especially at high temperature, their proton conductivities are significantly lower than that of hydrated sulfonic acid. When the acidic PS-PA particles and the basic PS-Tri particles were blended and hot-pressed into the acid-base composite membrane, a heterogeneous system is formed. Though we could not exclude the possible formation of a homogeneous system, hot-pressing the blend of PS-PA particles and PS-Tri particles below their melting points was more likely to result heterogeneous system, and a heterogeneous system was consistent with (or not contradict to) the SEM observation (**Figure 10a**).
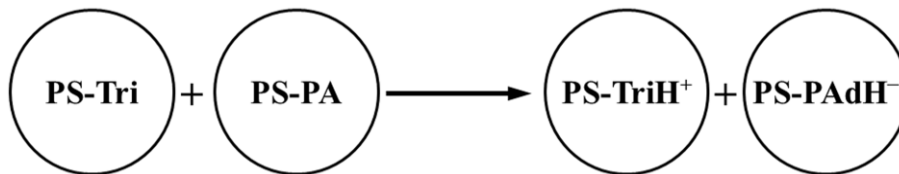
Furthermore, the heterogeneous system could be depicted by a percolating mosaic-like morphology model consisting of acidic PS-PA domains and basic PS-Tri domains (**Figure 10b**).[39, 40] At the domain interfaces, protons transport from the phosphonic acid groups to the triazolyl groups because of the acid-base neutralization reaction, and an acid-base equilibrium as well as space-charge layers are established between the PS-PA domains and the PS-Tri domains. At the equimolar mixing regions (domains), all the phosphonic acid groups and the triazolyl groups are depleted in the acid-base neutralization reaction, and a polymeric salt is formed. In the center of the PS-PA domains where the PS-PA and PS-Tri are blended at a molar ratio of more than 1 : 1, only the triazolyl groups are depleted and phosphonic acid groups remain. Besides the equimolar domains and PS-PA domains, there exist transition domains, PS-PAdH$^-$ domains from deprotonation of PS-PA and PS-TriH$^+$ domains from protonation of PS-TriH, because of the neutralization reaction between PS-PA and PS-Tri as pictorialized in **Figure 10c**.

SEM MAG: 10.00 kx   DET: SE Detector
HV: 20.0 kV   DATE: 01/13/14   5 um   Vega ©Tescan
VAC: HiVac   Device: TS5136MM   Digital Microscopy Imaging

(a)

(b)

(c)

Figure 10. (a) SEM of the cross-section of the membrane (the membrane was bent and broken quickly after being taken from liquid nitrogen). (b) The mosaic-like morphology model of the acid-base composite consists of PS-PA domains (yellow), deprotonated PS-PAdH$^-$ domains (black), and protonated PS-TriH$^+$ domains (red), and space-charge layers (white dots represent the negative charges, blue dots the positive charges) are formed at the domain interfaces. (c) Pictorialization of the acid-base neutralization reaction between the PS-PA and PS-Tri and the

formation of PS-PAdH$^-$ domains and PS-TriH$^+$ domains.

The formation of mosaic-like morphology causes the redistribution of charge carriers and increases the concentration of charge carriers at the domain interfaces and improves the overall conductivities of the membranes. This improvement of overall conductivities is similar to the space-charge effect in the heterogeneously doped systems or in the heterojunctions of the two-phase systems.[41-43] In the heterojunctions composed of CaF$_2$ and BaF$_2$, the ionic conductivity is improved for about two orders of magnitude attributing to the redistribution of fluoride ions at the interfaces.[41] As a matter of fact, the ionic conductivity of a two-phase mixture may exceed those of pure constituent phases even if the second phase is a "chemically inert" phase as alumina and silica.[43] The conductivity in heterogeneously doped systems or heterojunctions increases with the decrease in sizes of the heterostructures or the heterojunctions.[41-43] In our PS-PA and PS-Tri blend, the domain sizes are in range of 0.5 μm (**Figure 10a**) within upper limit of the heterojunctions of CaF$_2$ and BaF$_2$.[41] However, CaF$_2$ and BaF$_2$ are hard materials with minor mutual solubility between CaF$_2$ and BaF$_2$, and the PS-PA and PS-Tri are soft matters and gradual transition interfaces are expected.[41] Therefore, the domain sizes at 0.5 μm in the PS-PA and PS-Tri blend might correspond to much smaller equivalent heterostructures compared to the heterojunctions of CaF$_2$ and BaF$_2$.

The mosaic-like morphology model is consistent with the temperature dependence of proton conductivity. By fitting the proton conductivity σ to the Arrhenius equation (**Figure 11a**),

$$\sigma = \sigma_0 \exp(-E_a / RT)$$

where R and T are gas constant and temperature, the activation energy E_a and preexponential factor σ_0 are obtained as summarized in **Table 3**. We noticed the publications by Watanabe, et

al. that the overall conductivity change with temperature follows the Vogel-Fulcher-Tammann equation in ionic liquid.[44, 45]   In our case, no significant improvement was observed if the Vogel-Fulcher-Tammann equation is used attributing to the nonlinear curving fitting and more parameters to be determined compared with the Arrhenius equation.

Based on the mosaic-like morphology model and space-charge effect, the overall conductivity is determined by the concentration of transportable protons (charge carriers) and the transport barrier in the domain interfaces.   The preexponential factor increases with the concentration of transportable protons, and the activation energy increases with the transport barrier.   In homogeneous systems, such as the pure PS-PA and PS-Tri systems, there are no domain interfaces and no space-charge effect, and the preexponential factor is low.   In a 50.0% PS-PA membrane, the volumes of acidic domains and basic domains are almost equivalent and phosphonic acid groups are readily neutralized by the triazolyl groups in the domain interfaces, the overall concentration of transportable protons is limited.   As more and more PS-PA component is blended into the composite, more and more PS-PA domains are left unneutralized and the overall concentration of transportable protons increases.   The overall concentration of transportable protons will increase until reaching a maximum value in the 71.4% PS-PA system, and then decreases as excessive PS-PA is blended into the system.   Correspondently, the preexponential factor increases from 7.11×10^{-2} mS cm^{-1} in the 50.0% PS-PA system to a maximum value of 2.44×10^{10} mS cm^{-1} in the 71.4% PS-PA system, and then decreases to 3.17×10^{9} mS cm^{-1} in the 75.0% PS-PA system (**Table 3**).

From **Table 3**, it could be seen that the transport barrier also increases with the increase of PS-PA content.   In a homogeneous system, all the transportable protons occupy potential wells with similar depths and need to overcome the same transport barrier or activation energy.   In a

heterogeneous system, the transportable protons occupy various potential wells (from shallow wells to deep wells), and the transport barrier a transportable proton is determined by the well depth it occupies. The transportable protons occupy shallow wells, and the untransportable protons occupy the deepest wells and are actually trapped. In the domain interfaces, there are a spectrum of potential wells with different depth, consistent with the observation in the CaF_2-BaF_2 heterostructures where there is continuous change in activation energy.[41] In a system with low overall concentration of transportable protons, only a small portion of protons occupy shallow wells and are transportable, most of the other protons occupy deep wells and are untransportable. As the concentration of transportable protons increases, the transportable protons occupy not only shallow wells but also deeper wells resulting higher overall transport barriers (**Table 3**). In a system with highest concentration of transportable protons, the overall transport barrier also reaches its highest value. Finally, the overall transport barrier decreases as the concentration of transportable protons decreases. Under the joint effect of concentration change of transportable protons and transport barrier change, the overall proton conductivity increases significantly as more and more PS-PA is blended into the heterogeneous system and reaches the maximum value in the 66.7% PS-PA system.
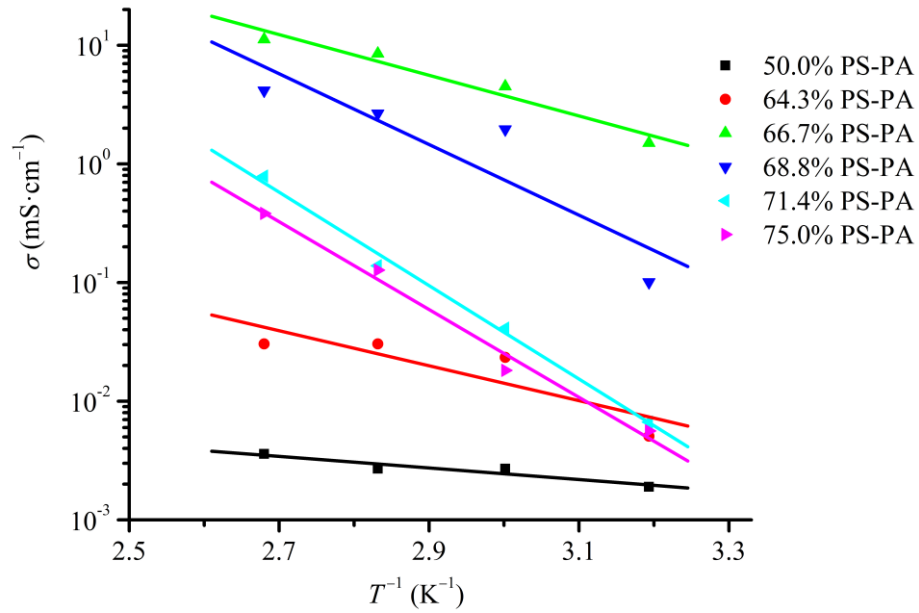
(a)
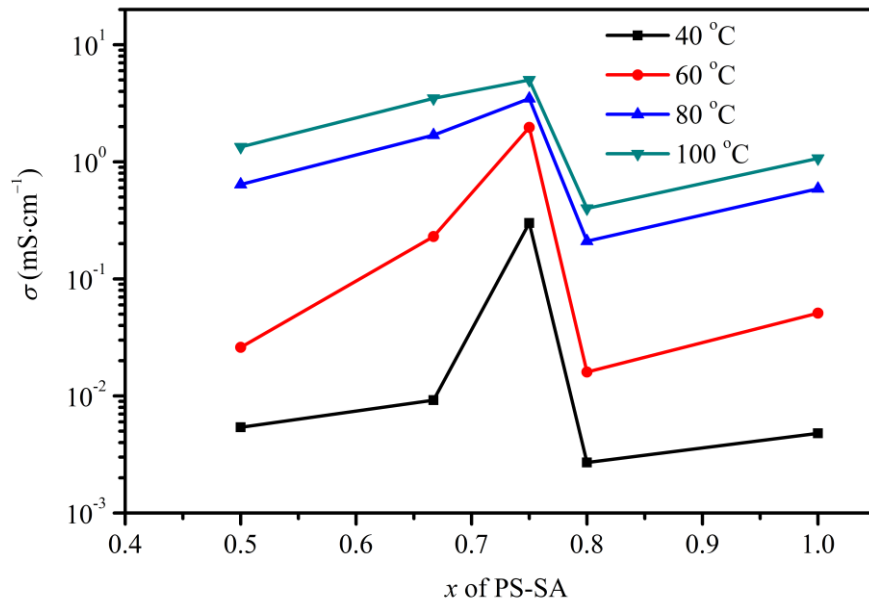
(b)

Figure 11. (a) Arrhenius plot for the proton conductivities of the PS-PA/PS-Tri composites. (b) The composites of PS-SA and PS-Tri also show synergetic proton conducting effect.

In order to verify if the synergetic proton conducting effect could be observed in other

acid-base composites, sulfonated polystyrene (PS-SA, the degree of sulfonation (DS) is 0.30) is synthesized and acid-base composites are prepared from PS-SA and PS-Tri. From the proton conductivity as shown in **Figure 11b**, it could be concluded that synergetic proton conducting effect is also observed in acid-base composites of PS-SA and PS-Tri, though not as great as that in the composites of PS-PA and PS-Tri.

Table 3. Activation energy and preexponential factor for the proton conductivity

Membranes	E_a (kJ mol^{-1})	σ_0 (mS cm^{-1})
50.0% PS-PA	9.34	7.11×10^{-2}
64.3% PS-PA	28.2	3.73×10^{3}
66.7% PS-PA	32.8	5.18×10^{5}
68.8% PS-PA	57.0	6.38×10^{8}
71.4% PS-PA	75.3	2.44×10^{10}
75.0% PS-PA	70.8	3.17×10^{9}

Nowadays, the most important method for the development of better proton conducting materials is to functionalize existing material with proton conducting groups, to modify structure of proton conducting materials, and to dope additives to existing material. However, the synergetic proton conducting effect allows us to develop better proton conducting materials by combination of different acidic polymers and basic polymers, and opens a new route to the development of new proton conducting materials.

4. CONCLUSION

In conclusion, acid-base composite proton exchange membranes were prepared from PS-PA and PS-Tri.　And the degree of phosphonation at 43% are significantly higher than that reported in literature at 33%,[35] and a degree of triazolylation at 60% is reported for the first time.

Synergetic proton conducting effect is observed in the acid-base composite proton exchange membrane composed of PS-PA and PS-Tri with a maximum proton conductivity of 11.2 mS cm^{-1} at 100 ℃ and RH 90%, three orders magnitude improvement compared to that of the acidic or basic component.　And the synergetic proton conducting effect is explained in terms of space-charge effect based on the mosaic-like morphology model consisting of free PS-PA domains, deprotonated PS-PAdH$^-$ domains, and protonated PS-TriH$^+$ domains.　In addition, the acid-base composite membrane shows reduced hydrophilicity with lowered water uptake of 15.1% (90 ^{o}C and 90% RH) and improved tensile strength at 16.3 MPa attributing to the ionic bridges between the acidic and basic components.

Finally, the synergetic proton conducting effect opens a new route to the development of new proton conducting materials by combination of different acidic and basic polymers.

ACKNOWLEDGMENTS

REFERENCES

[1]   A. B. Stambouli, Fuel cells: The expectations for an environmental-friendly and sustainable source of energy.   Renew. Sust. Energ. Rev. **2011**, 15(9): 4507-4520.

[2]   P. Costamagna and S. Srinivasan, Quantum jumps in the PEMFC science and technology from the 1960s to the year 2000:   Part I. Fundamental scientific aspects.   J. Power Sources **2001**, 102(1-2): 242-252.

[3]   P. Costamagna and S. Srinivasan, Quantum jumps in the PEMFC science and technology from the 1960s to the year 2000 Part II. Engineering, technology development and application aspects.   J. Power Sources **2001**, 102(1-2): 253-269.

[4]   B. Blunier and A. Miraoui, Proton exchange membrane fuel cell air management in automotive applications.   J. Fuel Cell Sci. Techn. **2010**, 7(4): 1007-1017.

[5]   L. Carrette, K. A. Friedrich, and U. Stimming, Fuel cells – Fundamentals and applications. Fuel Cells **2001**, 1(1): 5-39.

[6]   P. Corbo, F. Migliardini, and O. Veneri, Lithium polymer batteries and proton exchange membrane fuel cells as energy sources in hydrogen electric vehicles.   J. Power Sources **2010**, 195(23): 7849-7854.

[7]   P. Corbo, F. E. Corcione, F. Migliardini, and O. Veneri, Experimental study of a fuel cell power train for road transport application.   J. Power Sources **2005**, 145(2): 610-619.

[8]   P. Corbo, F. Migliardini, and O. Veneri, An experimental study of a PEM fuel cell power train for urban bus application.   J. Power Sources **2008**, 181(2): 363-370.

[9]   K. D. Kreuer, On the development of proton conducting polymer membranes for hydrogen and methanol fuel cells.   J. Membr. Sci. **2001**, 185(1): 29-39.

[10] S. J. Peighambardoust, S. Rowshanzamir, and M. Amjadi, Review of the proton exchange membranes for fuel cell applications.   Int. J. Hydrogen Energy **2010**, 35(17): 9349-9384.

[11] S. Bose, T. Kuila, T. X. H. Nguyen, N. H. Kim, K. T. Lau, and J. H. Lee, Polymer membranes for high temperature proton exchange membrane fuel cell: Recent advances and challenges.   Prog. Polym. Sci. **2011**, 36(6): 813-843.

[12] H. Zhang and P. K. Shen, Recent development of polymer electrolyte membranes for fuel cells.   Chem. Rev. **2012**, 112(5): 2780-2832.

[13] C. Yang, P. Costamagna, S. Srinivasan, J. Benziger, and A. B. Bocarsly, Approaches and technical challenges to high temperature operation of proton exchange membrane fuel cells. J. Power Sources **2001**, 103(1): 1-9.

[14] R. Savinell, E. Yeager, D. Tryk, U. Landau, J. Wainright, D. Weng, K. Lux, M. Litt, and C. Rogers, A polymer electrolyte for operation at temperatures up to $200^{o}C$.   J. Electrochem. Soc. **1994**, 141(4): L46-L48.

[15] P. Jannasch, Recent developments in high-temperature proton conducting polymer electrolyte membranes.   Curr. Opin. Colloid Interface Sci. **2003**, 8(1): 96-102.

[16] H. Zhang and P. K. Shen, Advances in the high performance polymer electrolyte membranes for fuel cells.   Chem. Soc. Rev. **2012**, 41(6): 2382-2394.

[17] S. Di, L. Yan, S. Han, B. Yue, Q. Feng, L. Xie, J. Chen, D. Zhang, and C. Sun, Enhancing the high-temperature proton conductivity of phosphoric acid doped poly(2,5-benzimidazole) by preblending boron phosphate nanoparticles to the raw materials.   J. Power Sources **2012**, 211: 161-168.

[18] A.-C. Dupuis, Proton exchange membranes for fuel cells operated at medium temperatures: Materials and experimental techniques.   Prog. Polym. Sci. **2011**, 56(3): 289-327.

[19] J. Ma, H.-J. Ni, D.-Y. Su, M.-Y. Huang, and X.-X. Wang, The research status of Nafion ternary composite membrane.   Int. J. Hydrogen Energy **2012**, 37(17): 13185-13190.

[20] S. Ü. Çelik, A. Bozkurt, and S. S. Hosseini, Alternatives toward proton conductive anhydrous membranes for fuel cells: Heterocyclic protogenic solvents comprising polymer electrolytes.   Prog. Polym. Sci. **2012**, 37(9): 1265-1291.

[21] Y. F. Liang, H. Y. Pan, X. L. Zhu, Y. X. Zhang, and X. G. Jian, Studies on synthesis and property of novel acid–base proton exchange membranes.   Chin. Chem. Lett. **2007**, 18(5): 609-612.

[22] Y. Fu, A. Manthiram, and M. D. Guiver, Blend membranes based on sulfonated poly(ether ether ketone) and polysulfone bearing benzimidazole side groups for proton exchange membrane fuel cells.   Electrochem. Commun. **2006**, 8(8): 1386-1390.

[23] M. Kufacı, A. Bozkurt, and M. Tülü, Poly(ethyleneglycol methacrylate phosphate) and heterocycle based proton conducting composite materials.   Solid State Ionics **2006**, 177(11-12): 1003-1007.

[24] D. Wu, T. Xu, L. Wu, and Y. Wu, Hybrid acid-base polymer membranes prepared for application in fuel cells.   J. Power Sources **2009**, 186(2): 286-292.

[25] I. Dimitrov, S. Takamuku, K. Jankova, P. Jannasch, and S. Hvilsted, Polysulfone functionalized with phosphonated poly(pentafluorostyrene) grafts for potential fuel cell applications.   Macromol. Rapid Commun. **2012**, 33(16): 1368-1374.

[26] M. Schuster, T. Rager, A. Noda, K. D. Kreuer, and J. Maier, About the choice of the protogenic group in PEM separator materials for intermediate temperature, low humidity operation: A critical comparison of sulfonic acid, phosphonic acid and imidazole functionalized model compounds.   Fuel Cells **2005**, 5(3): 355-365.

[27] S. J. Paddison, K. D. Kreuer, and J. Maier, About the choice of the protogenic group in polymer electrolyte membranes: Ab initio modelling of sulfonic acid, phosphonic acid, and imidazole functionalized alkanes.   Phys. Chem. Chem. Phys. **2006**, 8(39): 4530-4542.

[28] K. D. Kreuer, A. Fuchs, M. Ise, M. Spaeth, and J. Maier, Imidazole and pyrazole-based proton conducting polymers and liquids.   Electrochim. Acta **1998**, 43(10-11): 1281-1288.

[29] B. Yue, L. Yan, S. Han, and L. Xie, Proton transport pathways in acid-base complex consisting of phosphonic acid group and 1,2,3-triazolyl group.   J. Phys. Chem. B **2013**, 117(26): 7941-7949.

[30] L. Yan and L. Xie, *Molecular dynamics simulations of proton transport in proton exchange membranes based on acid-base complexes*, in *Molecular Interaction*, A. Meghea, Editor 2012, InTech: Rijeka, Croatia. p. 335-360.

[31] D. Zhang and L. Yan, Probing the acid-base equilibrium in acid-benzimidazole complexes by ^{1}H NMR spectra and density functional theory calculations.   J. Phys. Chem. B **2010**, 114(38): 12234-12241.

[32] S. Isikli, S. Tuncagil, A. Bozkurt, and L. Toppare, Immobilization of invertase in a novel proton conducting poly(vinylphosphonic acid)-poly(1-vinylimidazole) network.   J. Macromol. Sci., Part A: Pure Appl. Chem. **2010**, 47(7): 639-646.

[33] A. Aslan and A. Bozkurt, Development and characterization of polymer electrolyte membranes based on ionical cross-linked poly(1-vinyl-1,2,4-triazole) and poly(vinylphosphonic acid).   J. Power Sources **2009**, 191(2): 442-447.

[34] O. Acar, U. Sen, A. Bozkurt, and A. Ata, Proton conducting membranes based on poly(2,5-benzimidazole) (ABPBI)-poly(vinylphosphonic acid) blends for fuel cells.   Int. J. Hydrogen Energy **2009**, 34(6): 2724-2730.

[35] S. Subianto, N. R. Choudhury, and N. K. Dutta, Palladium-catalyzed phosphonation of SEBS block copolymer.   J. Polym. Sci. Part A: Polym. Chem. **2008**, 46(16): 5431-5441.

[36] N. Y. Abu-Thabit, S. A. Ali, and S. M. Javaid Zaidi, New highly phosphonated polysulfone membranes for PEM fuel cells.   J. Membr. Sci. **2010**, 360(1-2): 26-33.

[37] B. Lafitte and P. Jannasch, Phosphonation of polysulfones via lithiation and reaction with chlorophosphonic acid esters.   J. Polym. Sci. Part A: Polym. Chem. **2005**, 43(2): 273-286.

[38] B. Lafitte, M. Puchner, and P. Jannasch, Proton conducting polysulfone ionomers carrying sulfoaryloxybenzoyl side chains.   Macromol. Rapid Commun. **2005**, 26(18): 1464-1468.

[39] R. A. Rozendal, T. H. Sleutels, H. V. Hamelers, and C. J. Buisman, Effect of the type of ion exchange membrane on performance, ion transport, and pH in biocatalyzed electrolysis of wastewater.   Water Sci. Technol. **2008**, 57(11): 1757-1762.

[40] T. Xu, Ion exchange membranes: State of their development and perspective.   J. Membr. Sci. **2005**, 263(1-2): 1-29.

[41] N. Sata, K. Eberman, K. Eberl, and J. Maier, Mesoscopic fast ion conduction in nanometre-scale planar heterostructures.   Nature **2000**, 408(6815): 946-949.

[42] J. Maier, Space charge regions in solid two phase systems and their conduction contribution — II Contact equilibrium at the interface of two ionic conductors and the related conductivity effect. Ber. Bunsenges. phys. Chem. **1985**, 89(4): 355-362.

[43] J. Maier, Space charge regions in solid two-phase systems and their conduction contribution—I. Conductance enhancement in the system ionic conductor-'inert' phase and application on $AgCl:Al_2O_3$ and $AgCl:SiO_2$. J. Phys. Chem. Solids **1985**, 46(3): 309-320.

[44] A. Noda, K. Hayamizu, and M. Watanabe, Pulsed-gradient spin-echo ^{1}H and ^{19}F NMR ionic diffusion coefficient, viscosity, and ionic conductivity of non-chloroaluminate room-temperature ionic liquids. J. Phys. Chem. B **2001**, 105(20): 4603-4610.

[45] H. Tokuda, K. Ishii, M. A. B. H. Susan, S. Tsuzuki, K. Hayamizu, and M. Watanabe, Physicochemical properties and structures of room-temperature ionic liquids. 3. Variation of cationic structures. J. Phys. Chem. B **2006**, 110(6): 2833-2839.